Cryogenic to High Temperature Exploration of 4H-SiC W-SBD

Maxime Berthou, Besar Asllani, Pierre Brosselard, Philippe Godignon

Cryogenic to High temperature exploration of 4H-SiC W-SBD

M. Berthou[1], B. Asllani[1], P. Brosselard[1], P. Godignon[2]
[1]Laboratoire Ampère, 69100 Villeurbanne, France
[2]Centro Nacional de Microelectronica, 08193, Bellatera (Barcelona), Espana
E-mail: maxime.berthou@gmail.com

Abstract. W-SBD show exceptional reliability from 200 to 500K, however, its barrier analysis has never been performed thoroughly down 81K. This paper shows our study of Schottky barrier and Richardson coefficient, both extracted for different temperature ranges. We observed fluctuation in function of the temperature. We analyse this phenomenon and compare it to literature for other barriers. Measurements of reverse characteristics up to 1200V have been performed from 81 to 450K. It confirms that partial ionization influence on the drift doping impacts on the barrier height.

Introduction

W-SBD and JBS have shown high temperature capability and reliability for spacial applications [1] superior to Ni or Ti-SBD. Their higher barrier provides lower leakage current with similar commutation capability [2] compared to Ni barrier diodes. Thanks to its chemical properties and temperature stability, Tungsten barrier shows exceptional uniformity on 4H-SiC. Recent works have proven the role of defects [3] in the creation of microscopic areas of lower barrier height. These areas will later create leakage current paths or deteriorate the reliability of the device. Some of these defects are inevitable on 4H-SiC commercial wafers but they don't seem to have such impact on W- SBD as on Ni-SBD at room temperature.

Tested Devices

On an entire 1.2kV commercial wafers, the fabrication of 4 mm2 devices at CNM commonly yield more than 80% of good diodes. At room temperature, these diodes present a barrier height of 1.25 eV, ideality factor under 1.05 and leakage current under 10uA at 1kV. Two devices (A and B) were selected after cautious screening of double barriers and reverse capability for the measurement. They were made in different batches with similar fabrication technologies [2] except that the device A termination is made of two aluminium implantations to create the JTE and field stopper (see figure 1), and device B's uses one implantation to create the JTE. Device A and B drift thickness and doping are of 12 µm $5x10^{15}$ cm-3 and 6 µm 10^{16} cm-3 respectively. The difference of drift thickness will not change the barrier characteristics but its lower doping can have an impact.

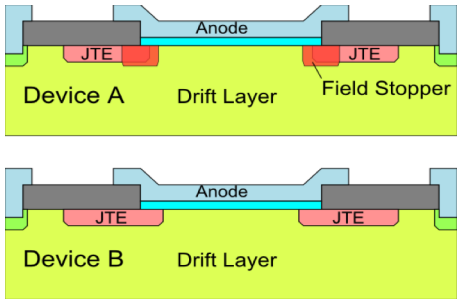

Fig. 1 – Schematic view of the structures of

Cryogenic measurement setup

Considering that BPD, TSD, etc. are in the density of more than 1000cm-2 on wafers of commercial quality, we theorized that the parallel barrier they cause is too close to the dominant barrier created by W/SiC interface and it is not perceptible in the IV curves at room temperature. In order to electrically characterize the Schottky barrier in a wide range of temperatures, we employed a cryogenic chamber under vacuum and cooled by liquid nitrogen presented in figure 2. This setup allows measuring the device from 81 to 500K with temperature precision of 1K. The electrical characteristics were captured with an Agilent B1505 equipped with high voltage, capacitance and current precision modules and connected to the device in the cryogenic chamber with coaxial cables. This tool allowed us to measure the forward current and leakage current with great precision down to 100pA, which is very important for barrier

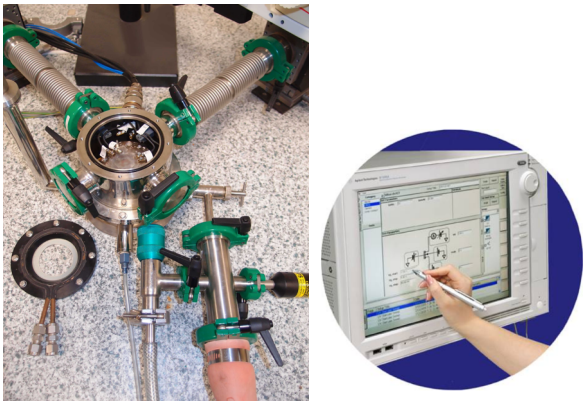

Fig. 2 – pictures of the measurement tool B1505 and

analysis for I-V measurements.

Measurement results

Considering the theory [4,5], if the Schottky contact is composed of areas of different barrier heights with different ratios, they will be more distinguishable at lower temperature. Our cryogenic I-V measurements of the W-SBD devices, shown in fig. 1, did not evidence the presence of multiple barriers at low temperature. This characterizes high degree of barrier homogeneity. We then based our analysis on this device with barrier of high quality. Until now, the W-SiC barrier analysis was performed at room or higher temperature. On various articles, difference between measurements and theory on SiC-SBD have often been attributed to Tung's model [4,5]. Such study has never been performed on W-SBD at low temperature and using samples of such quality allows us to explore it.

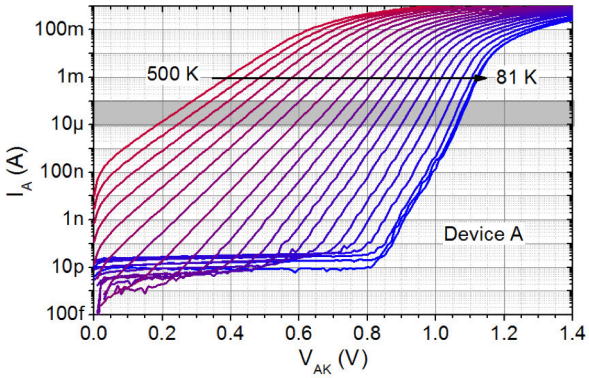

Fig. 3 – Direct characteristics in logarithmic scale representation for device A on wide temperature range from 81 to 500 K

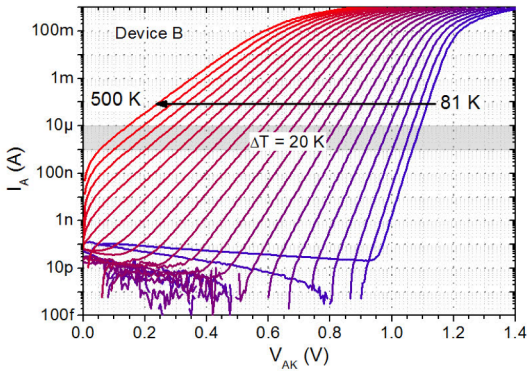

Fig. 4 – Direct characteristics of device B on wide temperature range from cryogenic to high temperature conditions

Forward IV characteristics

For devices A and B, IV characteristics were measured from 81 to 500 K every 20 K as shown in figure 3 and 4. We can see that no double barrier is perceivable down to 81 K, which shows its purity and presents an ideal case for barrier analysis from I-V curves. As the I-V curve evolves a lot with temperature, it is difficult to choose the voltage or current criteria to extract the different physical parameters such as barrier height (ΦB), ideality factor (η) and Richardson coefficient (A*).

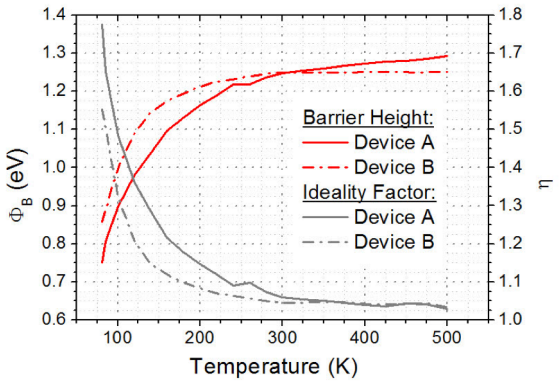

Fig. 5 – Barrier heigh and ideality factor extracted from I-V characteristics between 10μA and 100μA on both devices

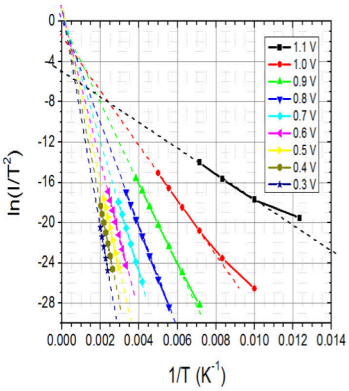

Fig. 6 – ln(I/T2) curves at various biases extracted from forward IV of device B to compute A* at various temperatures

Two methods were used and compared on the two devices; the first one consists in choosing several voltages around which to perform the regression and extract η and ΦB in order to sweep through the whole range of temperatures as shown in figure 5. The second one consists in choosing a current range, as shown by the greyed area in figure 3 and 4, in which to perform the regression in order to measure η and ΦB for each temperature. The figure 5 shows the results obtained with the second method. We can see that the second method provides more uniform results and is more appropriate for this analysis. At temperatures under 250K, the barrier height decreases and the ideality factor increases, this effect is linked to the partial ionization effect which decreases the effective drift doping concentration and thus

reduces the barrier quality.

By manipulating the thermionic equation 1 of Schottky current and neglecting the partial ionization

$$J = A^{**}T^2\frac{N_d^+}{N_c}\exp\left(-\frac{q\Phi_{B,n}}{kT}\right)\left[\exp\left(\frac{qV}{nkT}\right)-1\right] \quad (1)$$

we obtain the equation 2, which allows us to extract Richardson coefficient. To do so, $ln(I/T^2)$ must be plotted in function of $1/T$ for a fixed voltage bias and the created affine function intersection yields $ln(SA^*)$ and thus the Richardson coefficient. In figure 6, we plotted $ln(I/T^2)$ curves for several voltage biases extracted from device B. The voltage biases correspond to different temperature ranges and we can note that A^* decreases together with the temperature as shown in figure 7.

$$\ln\left(\frac{J}{T^2}\right) = \frac{q}{k_BT}\left(\frac{V}{n}-\phi_B\right)\frac{1}{T}+\ln(A^*) \quad (2) \qquad \ln\left(\frac{J}{T^2}\right) = \frac{q}{k_BT}\left(\frac{V}{n}-\phi_B\right)\frac{1}{T}+\ln\left(\frac{N_d^+}{N_c}A^*\right) \quad (3)$$

In the equation 2, partial ionization is neglected and taking it into account yields the equation 3; as the temperature decreases and N_D^+/N_C decreases, the intersection with y axe should decrease, which is the phenomenon observed in figure 6 and reflected in the extracted Richardson coefficient in figure 7. This shows that the partial ionization phenomena must be taken into account for the analysis of the Schottky barrier at low temperature. More detailed studies of the theory behind this effect are currently performed to explain it scientifically.

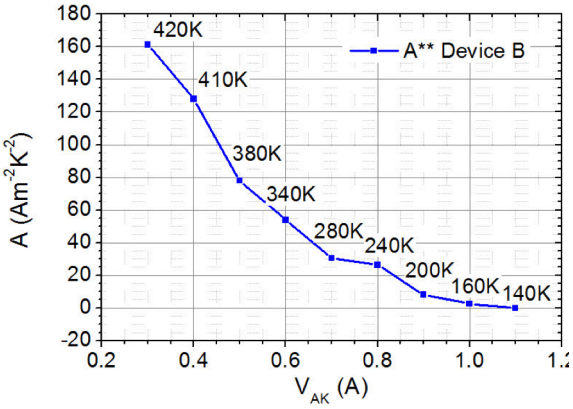

Fig. 7 – Extracted Richardson values from ln(I/T2) graph for the different voltage biases for device B

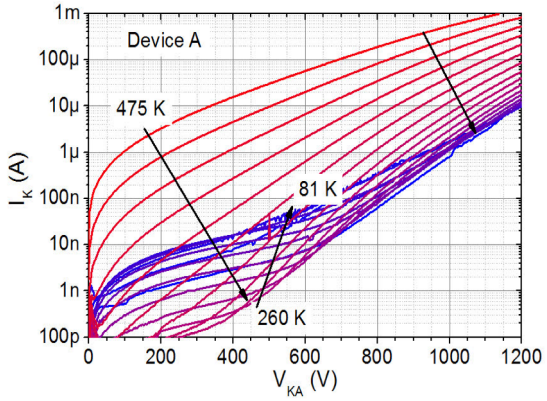

Fig. 8 – Reverse characteristics of device A up to 1200V from 475 K down to 81 K

Reverse IV characteristics

As the partial ionization may have strong impact on reverse characteristics, we measured it up to 1.2kV for device A (see figure 8) and 400V for device B (see figure 9) from 81 to 480 K. Both measurements have shown unusual effects at low temperatures. When temperature decreases below 260 K, we can observe an increase of the leakage current under 800V. As the barrier height decreases, the leakage current increases and this phenomena becomes dominant under 260 K. At higher voltage bias, we can note that the leakage current behaviour changes, as it is constant under 260K. This second phenomenon might be explained by the influence of depletion area on the partial ionization or termination issues due to interficial traps over the JTE. The partial ionization can explain the barrier degradation at low temperature shown in figure 5, which shows stronger effect on the barier height of Device A compared to Device B. If this hypothesis is valid, it may explain the leakage current behavior at low temperature. This phenomenon is less visible on device B as shown in

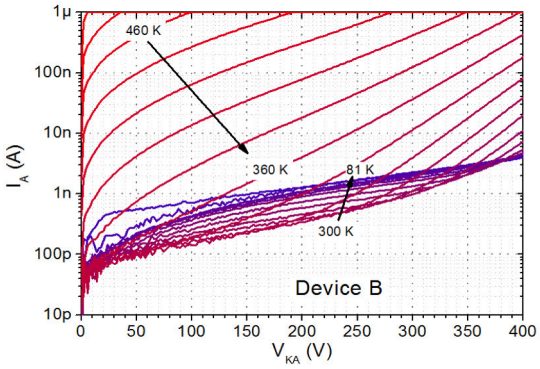

Fig. 9 – Reverse characteristics of device B up to 400 V from 480 K down to 81 K

figure 9. The partial ionization can still explain the difference; as the impurity concentration is one order of magnitude higher, the partial ionization cannot lower the effective doping concentration as low as in device A and the barrier quality suffers less from it. Concerning the interficial traps over the termination, we know that their density increases at lower temperature and the leakage channel may be enhanced we the temperature decreases as shown in figure 8 and 9.

Capacitive Measurements have been performed on device B to extract the effective drift layer concentration at different temperatures from 300 to 81 K as presented in figure 10. Taking the incomplete ionization equation from [6] and expressing it in function of the carrier concentration instead of the quazi-fermi level, we obtain the equation 3. In the depleted area, free carrier concentration tends toward 0 thus N_D^+ increases toward $N_{D,0}$. Classical formula used here (see equation 4) to calculate of the doping concentration, does not take the partial ionization into account, which produces an increasing drift doping profile with voltage bias instead of a constant one.

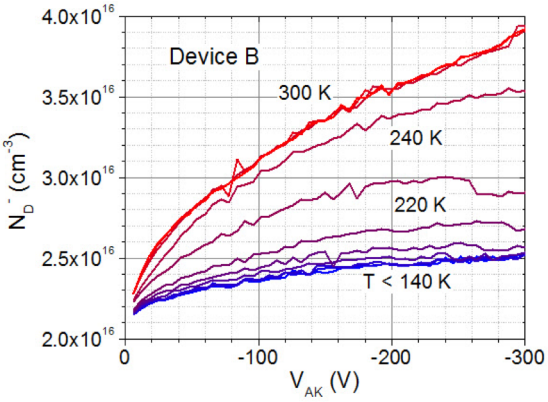

Fig. 10 – Effective drift doping level calculated from C-V measurements on device B.

$$N_D^+ = \frac{N_{D,0}}{1 + g_D \frac{n}{Nc} exp\left(\frac{\Delta E_D}{k_B T}\right)} \quad (4)$$

$$N_D^+ = \frac{2}{q\epsilon_{SiC}\epsilon_0 A^2 \frac{d(1/C^2)}{dV}} \quad (5)$$

Nonetheless, in figure 10, we can see the temperature influence on the measured effective drift doping as the doping stays constant from 300 down 260 K, then decreases and stabilizes at 140 K. This stabilization is questioning, further theoretical studies and more measurements are required to confirm and explain this phenomenon. However, these temperatures correspond well with the reverse leakage current temperature thresholds observed on both devices in figures 8 and 9.

Conclusion

Characterisations of W-SBD at cryogenic temperatures allowed us to study its barrier physics and fundamental parameters on an extended temperature range. High voltage measurements have evidenced the presence of a second current leakage mechanism and two hypothesis have been stated to explain it. Further measurements and analysis are required to validate one of the theories. Extracted doping concentration from capacitance measurement has also shown strong dependency with temperature and incomplete ionization can also explain such behaviour. All measurement tend to show that incomplete ionization has a strong impact of the different characteristics of the SiC device and taking it more into account may help better modelize the Schottky devices.

Acknowledgements

This study was funded by PEA-DGA MADASIC project.

[1] P. Godignon, X. Jorda, M. Vellvehi, X. Perpina, V. Banu, D. Lopez, S. Massetti, *Industrial Electronics, IEEE Transactions on*, *58*(7), 2582–2590 (2011).
[2] M. Berthou, P. Godignon, J. Montserrat, J. Millan and D. Planson, *Journal of Electronic Materials*, *40*(12), 2355–2362 (2011).
[3] K.-Y. Lee and Y.-H. Huang, *IEEE Transactions on Electron Devices*, *59*(3), 694–699 (2012).
[4] M. Zaman, D. Perrone, S. Ferrero, L. Scaltrito and M. Naretto, *Materials Science Forum,* Vol. 711, pp. 174–178, (2012).
[5] Tung, R. T.,*Materials Science and Engineering: R: Reports*, *35*(1-3), 1–138 (2001).